JOURNAL OF VIROLOGY, June 2010, p. 6208–6217 Vol. 84, No. 12
0022-538X/10/$12.00 doi:10.1128/JVI.00317-10

Dimeric Architecture of the Hendra Virus Attachment Glycoprotein: Evidence for a Conserved Mode of Assembly▽†

Thomas A. Bowden,[1] Max Crispin,[2] David J. Harvey,[2] E. Yvonne Jones,[1] and David I. Stuart[1,3]*

Division of Structural Biology, Wellcome Trust Centre for Human Genetics, University of Oxford, Roosevelt Drive, Oxford OX3 7BN, United Kingdom[1]; Oxford Glycobiology Institute, Department of Biochemistry, University of Oxford, South Parks Road, Oxford OX1 3QU, United Kingdom[2]; and Science Division, Diamond Light Source Ltd., Diamond House, Harwell Science and Innovation Campus, Didcot, Oxfordshire 0X11 0DE, United Kingdom[3]

Received 10 February 2010/Accepted 25 March 2010

Hendra virus is a negative-sense single-stranded RNA virus within the *Paramyxoviridae* family which, together with Nipah virus, forms the *Henipavirus* genus. Infection with bat-borne Hendra virus leads to a disease with high mortality rates in humans. We determined the crystal structure of the unliganded six-bladed β-propeller domain and compared it to the previously reported structure of Hendra virus attachment glycoprotein (HeV-G) in complex with its cellular receptor, ephrin-B2. As observed for the related unliganded Nipah virus structure, there is plasticity in the Glu579-Pro590 and Lys236-Ala245 ephrin-binding loops prior to receptor engagement. These data reveal that henipaviral attachment glycoproteins undergo common structural transitions upon receptor binding and further define the structural template for antihenipaviral drug design. Our analysis also provides experimental evidence for a dimeric arrangement of HeV-G that exhibits striking similarity to those observed in crystal structures of related paramyxovirus receptor-binding glycoproteins. The biological relevance of this dimer is further supported by the positional analysis of glycosylation sites from across the paramyxoviruses. In HeV-G, the sites lie away from the putative dimer interface and remain accessible to α-mannosidase processing on oligomerization. We therefore propose that the overall mode of dimer assembly is conserved for all paramyxoviruses; however, while the geometry of dimerization is rather closely similar for those viruses that bind flexible glycan receptors, significant (up to 60°) and different reconfigurations of the subunit packing (associated with a significant decrease in the size of the dimer interface) have accompanied the independent switching to high-affinity protein receptor binding in Hendra and measles viruses.

The zoonotic Hendra virus (HeV) uses the flying fox as a natural host and is highly virulent in humans and horses. Reported cases of HeV transmission in humans have, to date, been sporadic and restricted to Australia (23, 32, 42). HeV was originally discovered in 1994 following the infection and subsequent death of a horse trainer and numerous horses (42, 49). Infection was characterized by the swift onset (7 to 10 days) of acute respiratory disease with clinical symptoms including fever, dizziness, hypotension, and respiratory illness. HeV is closely related to Nipah virus (NiV) which, in its largest outbreak, was responsible for the death of approximately 105 people in Malaysia (46). HeV and NiV (referred to as HNV) collectively form the *Henipavirus* genus which belongs to the *Paramyxoviridae* family of single-stranded, negative-sense RNA viruses. Putative new members of this genus have been recently identified in African bats (19).

HeV contains attachment (HeV-G) and fusion (HeV-F) membrane glycoproteins which extend from the viral envelope and are required for efficient entry (20). HeV and NiV exhibit a broad tissue tropism which correlates with the use of the widely expressed cell surface glycoproteins ephrin-B2 (EFNB2) and ephrin-B3 (EFNB3) as functional receptors for HeV-G and NiV-G (referred to as HNV-G). Oligomerization of HeV-G is also critical for productive attachment (1, 4). Despite the shared underlying molecular architecture of the attachment glycoprotein across the paramyxoviruses, there is marked divergence in their cellular receptors. Newcastle disease virus (NDV) and parainfluenza viruses (PIVs) attach to cell surface sialic acid (neuraminic acid), a negatively charged nine-carbon saccharide that is located at the nonreducing termini of glycolipids and N- and O-linked glycans of glycoproteins. In contrast, morbilliviruses such as measles virus (MV), canine distemper virus, and rinderpest virus have been shown to require surface lymphocyte activation molecule (SLAM; CD150) (51, 52) or the complement regulator CD46 for viral attachment (18, 44, 48). Structure-based phylogenetic analysis of available paramyxovirus structures shows that NiV-G and HeV-G are structurally more similar to attachment glycoproteins of sialic acid-binding viruses such as NDV and PIVs than to that of MV (7). We have suggested that the protein-binding capacities of henipaviruses and morbilliviruses have evolved independently, indicating an innate propensity for viruses to acquire novel protein receptor specificity, a characteristic that presents a natural route for the emergence of new pathogenic viruses (7).

HeV-G and NiV-G are closely related by sequence (81% identity) and structure (7). This similarity is underscored by the ob-

* Corresponding author. Mailing address: Division of Structural Biology, Wellcome Trust Centre for Human Genetics, University of Oxford, Roosevelt Drive, Oxford OX3 7BN, United Kingdom. Phone: 44 01865 287 546. Fax: 44 01865 287 547. E-mail: dave@strubi.ox.ac.uk.

† Supplemental material for this article may be found at http://jvi.asm.org/.

▽ Published ahead of print on 7 April 2010.

servation that vaccination of cats with recombinant HeV-G can protect against challenge with NiV (39). The similarity is evident in the crystal structures of NiV-G and HeV-G in complex with EFNB2, which both display a common binding mode (7). Knowledge of the molecular determinants of HeV attachment and fusion is of value for the rational development of immunotherapeutic and antiviral reagents with which to target these viruses. Such a structure-based approach to drug design has led to the development of active antivirals against influenza (2). However, in contrast to the rigid carbohydrate binding cleft of influenza neuraminidase, crystallographic analysis of the unbound NiV-G revealed significant plasticity in many of the EFNB2-binding loops which extend from the β-propeller scaffold (10). This information redefines the structural template for rational antiviral drug design against the HNV-G family of viral glycoproteins. Here, we have sought to further refine this template by identifying structural characteristics of HeV attachment.

We have crystallized and solved the structure of the globular six-bladed β-propeller domain of HeV-G. Analysis of this structure reveals that, as previously observed for the closely related NiV-G, significant conformational changes occur in the EFNB2 and EFNB3 receptor binding loops between unliganded and receptor-bound structures (10). Additionally, based on the packing of identical HeV-G molecules in the crystal asymmetric unit, we provide a model for the dimeric component of the native oligomeric assembly of the attachment glycoprotein. This model is consistent with oligomeric structures from other paramyxovirus attachment glycoproteins, and we propose that it may represent a component of the biological assembly. Furthermore, we observe that the angle of association between monomeric subunits is much more conserved between glycan-binding hemagglutinin-neuraminidases (HN) than the protein-binding HeV and MV attachment glycoproteins. As a result, we suggest that the acquisition of protein-binding functionality by paramyxoviruses may require structural adaptation, which perturbs the conserved dimeric packing. Together these data support the hypothesis of a globally conserved mode of oligomerization among the paramyxoviruses.

MATERIALS AND METHODS

Protein expression and purification. Full-length soluble ectodomain of HeV-G (HeV-G_{ecto}; residues 71 to 604, GenBank accession number NC_001906; cDNA synthesized by GeneArt, Regensburg, Germany) and the β-propeller domain (HeV-G_{β}; residues 183 to 604) were cloned into the pHLsec vector and transiently expressed in human embryonic kidney (HEK) 293T cells (ATCC CRL-1573) and purified as previously described (3, 7–10, 14). Transient transfections were performed using 2 mg DNA per liter cell culture. When used, the α-mannosidase inhibitor kifunensine (Cayman Europe, Tallinn, Estonia) was added at the stage of transfection to a concentration of 5 μM (11, 14). Glycoprotein was purified by immobilized metal affinity chromatography and then treated with *Flavobacterium meningosepticum* endoglycosidase (endo) F_1 (75 μg mg^{-1} protein; 12 h; 21°C) which hydrolyzes the glycosidic linkage of the di-*N*-acetylchitobiose core of oligomannose-type N-linked glycans. Following deglycosylation, proteins were purified by size exclusion chromatography (SEC) using a Superdex 200 10/30 column (Amersham, United Kingdom) in 150 mM NaCl, 10 mM Tris (pH 8.0) buffer. Typical pure glycoprotein yields per liter of cell culture were approximately 1.0 mg for glycosylated HeV-G_{ecto} and 0.75 mg of deglycosylated HeV-G_{β}.

Crystallization and structure determination. Crystals were grown by sitting drop vapor diffusion using 100 nL protein plus 100 nL precipitant as described previously (54). HeV-G crystals grew at 4°C (5.8 mg ml^{-1}) in 30% PEG 8000 (wt/vol), 0.2 M ammonium sulfate, and 0.1 M sodium cacodylate buffer (pH 6.5) after 49 days. Crystals were flash frozen by immersion in a cryoprotectant containing 25% (vol/vol) glycerol followed by rapid transfer to a gaseous nitrogen stream. Data were collected at Beamline ID23-2 at the European Synchrotron Radiation Facility (ESRF), Grenoble, France. Images were integrated and scaled using the programs HKL2000 and Scalepack (45). Details are presented in Table 1. The structure of HeV-G was solved by molecular replacement using the program Phaser (38) with unbound NiV-G (Protein Data Bank [PDB] accession number 2VWD) as the search model. Four molecules were identified in the asymmetric unit. Structure refinement was performed using Refmac 5 in the CCP4 suite and included iterative restrained refinement with TLS modeling and tight main chain and loose side chain noncrystallographic symmetry restraints between the four HeV-G molecules in the asymmetric unit (43, 56). The program COOT was used for manual rebuilding (22), and Molprobity was used to validate the model (17). Structural alignments were performed with the program SHP (50), and molecular graphics images were generated using PyMOL (DeLano Scientific, San Carlos, CA).

Mass spectrometry of oligosaccharides. Glycans were released enzymatically following the method of Küster et al. (34). Coomassie blue-stained SDS-PAGE bands containing approximately 10 μg of target HeV glycoproteins were excised,

TABLE 1. Crystallographic data and refinement statistics for HeV-G

Parameter[a]	Value[b]
Data collection	
Resolution (Å)	50.0–2.90 (2.95–2.90)
Space group	*P*1
Cell dimensions	
a, *b*, *c* (Å)	65.8, 84.6, 91.4
α, β, γ (°)	91.4, 103.4, 108.8
Wavelength (Å)	0.873
Unique reflections	38,664 (1,946)
Completeness (%)	99.2 (98.0)
R_{merge} (%)[c]	16.6 (44.7)
I/σI	6.1 (2.0)
Avg redundancy	3.0 (2.9)
Refinement	
Resolution range (Å)	50.0–2.90 (2.97–2.90)
No. of reflections	36,735 (2,541)
R_{work} (%)[d]	23.3
R_{free} (%)[e]	27.3
RMSD	
Bond (Å)	0.008
Angle (°)	1.1
Main chain bond *B* factor (Å^2)	0.7
Side chain bond *B* factor (Å^2)	1.0
Between NCS-related Cα atoms (Å)	0.3
Molecules per ASU	4
Atoms per ASU (protein/carbohydrate/water)	13,207/140/117
Avg *B* factors (Å^2) (protein/carbohydrate/water)	28.3/16.6/18.5
Model quality (Ramachandran plot)[f]	
Most favored region (%)	95.0
Allowed region	5.0

[a] Data were collected at Beamline ID23-EH2 at the ESRF (Grenoble, France). RMSD, root mean square deviation from ideal geometry; NCS, noncrystallographic symmetry; ASU, asymmetric unit.

[b] Numbers in parentheses refer to the relevant outer resolution shell.

[c] $R_{merge} = \Sigma_{hkl} \Sigma_i |I(hkl;i) - \langle I(hkl)\rangle| / \Sigma_{hkl} \Sigma_i I(hkl;i)$, where $I(hkl;i)$ is the intensity of an individual measurement and $\langle I(hkl)\rangle$ is the average intensity from multiple observations.

[d] $R_{work} = \Sigma_{hkl} ||F_{obs}| - k|F_{calc}|| / \Sigma_{hkl} |F_{obs}|$.

[e] R_{free} is calculated as for R_{work} but using only 5% of the data that were sequestered prior to refinement.

[f] Ramachandran plots were calculated with Molprobity (17).

washed with 20 mM $NaHCO_3$, pH 7.0, and dried in a vacuum centrifuge before rehydration with 30 μl of 30 mM $NaHCO_3$ (pH 7.0) containing 100 units ml^{-1} of protein *N*-glycanase F (PNGase F) (Prozyme, San Leandro, CA). After incubation for 12 h at 37°C, the enzymatically released N-linked glycans were eluted with water and the sample was passed through a 0.45-μm-pore-size filter (Millex-LH, hydrophobic polytetrafluoroethylene). Aqueous solutions of the glycans were cleaned with a Nafion 117 membrane (5).

Positive ion matrix-assisted laser desorption ionization–time of flight (MALDI-TOF) mass spectra were recorded with a Shimazu AXIMA performance MALDI-TOF/TOF mass spectrometer fitted with delayed extraction and a nitrogen laser (337 nm). Samples were prepared by adding 0.5 μl of an aqueous solution of the glycans to the matrix solution (0.3 μl of a saturated solution of 2,5-dihydroxybenzoic acid in acetonitrile) on the stainless steel target plate and allowing it to dry at room temperature. The sample/matrix mixture was then recrystallized from ethanol. Further samples were examined after removal of sialic acids by heating at 80°C for 1 h with 1% acetic acid.

Electrospray mass spectrometry (MS) was performed with either a Waters quadrupole-time of flight (Q-TOF) Ultima Global instrument or a Q-TOF model 1 spectrometer (Waters MS Technologies, Manchester, United Kingdom) in negative-ion mode. Samples in 1:1 (vol/vol) methanol/water were infused through Proxeon nanospray capillaries (Proxeon Biosystems, Odense, Denmark). The ion source conditions were as follows: temperature, 120°C; nitrogen flow, 50 liters h^{-1}; infusion needle potential, 1.1 kV; cone voltage, 100 V; RF-1 voltage, 150 V (Ultima Global instrument). Spectra (2-s scans) were acquired with a digitization rate of 4 GHz and accumulated until a satisfactory signal-to-noise ratio had been obtained. For MS/MS data acquisition, the parent ion was selected at a low resolution (a mass window of about 5 *m/z*) to allow transmission of isotope peaks and fragmented with argon at a pressure of 0.5 mBar. The voltage on the collision cell was adjusted to give an even distribution of fragment ions across the mass scale. Typical values were 80 to 120 V. Other voltages were as recommended by the manufacturer. Instrument control, data acquisition, and processing were performed with MassLynx (Waters) software version 4.0 (Q-TOF 1) or 4.1 (Ultima Global). Analysis of fragmentation spectra was performed as previously described (25–28, 30).

Protein Data Bank accession number. Coordinates and structure factors have been deposited in the Protein Data Bank under accession number 2X9M.

RESULTS AND DISCUSSION

Expression of oligomeric and monomeric HeV-G. The full-length soluble region of HeV-G (HeV-G_{ecto}; residues 71 to 604) and the globular six-bladed β-propeller domain (HeV-G_β; residues 183 to 604) of HeV-G were transiently expressed in HEK 293T cells. The glycoproteins contained a C-terminal hexahistidine tag to facilitate metal affinity purification. The HeV-G β-propeller domain elutes as a monomeric species on size exclusion chromatography (Fig. 1A and B). In contrast, HeV-G_{ecto}, containing the N-terminal stalk region, was a mixture of putative dimeric and tetrameric states (Fig. 1C and D). These observations are consistent with a previous analysis of HeV-G_{ecto} by Bossart et al. (6) and studies of related PIV3 and PIV5 hemagglutinin-neuraminidases, which have demonstrated that the β-propeller domain alone does not display oligomerization in solution-state measurements (35, 58, 59). Furthermore, negative-stain electron microscopic studies revealed similar oligomeric and monomeric species for the full-length ectodomain and isolated β-propeller domain of PIV5-HN, respectively (58). These observations also mirror our previous analysis of the β-propeller domain of NiV-G (NiV-G_β) by analytical ultracentrifugation in which only monomeric species were detected (7). In contrast, equivalent analysis of the full-length ectodomain of NiV-G revealed putative tetrameric species (7).

The glycosylation of HeV-G_β was manipulated to promote crystallogenesis (11). HeV-G_β was expressed in the presence of the α-mannosidase inhibitor, kifunensine. Kifunensine inhibits both endoplasmic reticulum (ER) α-mannosidase I and the Golgi α-mannosidases IA to C and consequently prevents processing of the nascent glycoproteins (15, 21). This inhibition traps the glycans as immature oligomannose-type compounds and renders them sensitive to cleavage by endo F_1 (11). Mass spectrometric analysis of glycosylation on equivalently expressed NiV-G_β confirmed that the glycans were mainly $Man_9GlcNAc_2$, although lower levels of the $Man_{5\text{-}8}GlcNAc_2$ were also detected (10). Following endo F_1 treatment, size exclusion liquid chromatography and SDS-PAGE analysis (Fig. 1A and B) suggested an approximate 15-kDa decrease in apparent molecular mass. This indicates that the recombinant oligomannose glycoform of HeV-G_β is composed of approximately 20% carbohydrate, consistent with the presence of five predicted N-linked glycosylation sequons.

Structure of unbound HeV-G. Crystals were generated of deglycosylated HeV-G_β, and the structure was determined to a resolution of 2.9 Å. The structure was solved by molecular replacement using the program Phaser (38) with the unbound structure of NiV-G_β (PDB accession number 2VWD) as the search model.

The crystallographic asymmetric unit contains four HeV-G molecules. As previously reported, HeV-G forms a six-bladed β-propeller fold (7). Each blade (β1 to β6) is composed of four antiparallel β-strands (S1 to S4), and the blades are assembled in a toroidal arrangement around a central axis (Fig. 2A). The ephrin-binding site is located across one face of the β-propeller fold perpendicular to the central axis (Fig. 2A). The globular β-propeller fold is stabilized by seven intrachain disulfide bonds, and the N and C termini extend in the same direction. The overall topology and disulfide bond pattern of the β-propeller is conserved with NiV-G (7, 10, 57).

The four molecules identified in the crystallographic asymmetric unit are very similar to each other and superpose with very small deviations (chains A to D; 0.3-Å root mean square [RMS] deviation in equivalent Cα position over 418 residues). In contrast to the previously reported structure of HeV-G in complex with EFNB2, the main chain atoms could be modeled into continuous electron density from residue Asn186 to Glu603. The electron density is improved for the ephrin-binding face (Tyr581 to Asp585) (Fig. 2B and C, region 1) and in the region of interaction between molecules within the asymmetric unit (Ser204 to Arg212) (Fig. 2B and C, region 2).

Structural comparison of bound and unbound HeV-G. Analyses of NiV-G alone and in complex with human cell surface receptors, EFNB2 and EFNB3, revealed significant rearrangements in the EFN-binding loops upon receptor recognition (10, 57), and a comparison of the unliganded HeV-G structures determined here with those in complex with EFNB2 also reveals significant plasticity around the Glu579-Pro590 loop (Fig. 2C, region 1). The observed conformational change in this region upon receptor engagement is consistent with an induced-fit mechanism for receptor binding, further emphasizing that the structures of both bound and apo forms of viral attachment glycoproteins must be considered when used as templates for structure-based design of antiviral drugs.

Structural comparison of unbound HeV-G with NiV-G. Superposition of unbound HeV-G and NiV-G structures shows that the receptor binding domains of the two glycoproteins are very similar (1.1-Å RMS deviation in equivalent Cα position over 410 residues) (Fig. 2B and C, region 3). Nevertheless, there are sig-

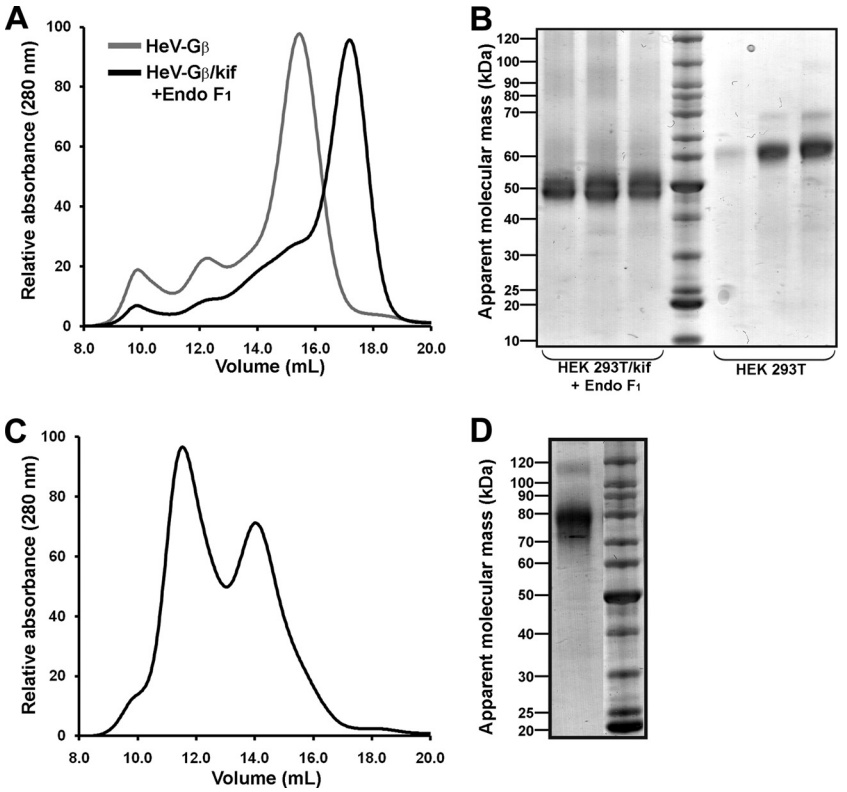

FIG. 1. Purification of HeV-GS_β and HeV-G_{ecto}. (A) Overlay of the elution profile of size exclusion chromatography using an S200 10/30 column of HeV-GS_β expressed with kifunensine (deglycosylated with endo F_1) (black line) and in the absence of kifunensine (gray line). (B) A 4 to 12% gradient SDS-PAGE of the resulting protein from size exclusion chromatography (C) run under reducing conditions. The middle lane shows molecular mass markers. (C) Size exclusion chromatography curve of HeV-G_{ecto} run on an S200 10/30 column. The two peaks correspond to HeV-G_{ecto}, which elutes as multiple oligomeric species. (D) A 4 to 12% gradient SDS-PAGE of the resulting pooled HeV-G_{ecto} from size exclusion chromatography (A) run under reducing conditions. The left lane shows pooled HeV-G_{ecto}, and the right lane shows molecular mass markers. The panel shows a merged image from two lanes of the same gel. Note that HeV-GS_β and HeV-G_{ecto} were purified on different, nonstandardized S200 10/30 columns, and as a result the relative size exclusion chromatography elution volumes from panels A and C are not comparable.

nificant structural differences in the Glu579-Pro590 EFN-binding loops. In the unbound HeV-G, this loop is elongated and extends toward the periphery of the β-propeller, while in NiV-G this region forms two antiparallel β-strands joined by a short loop (Fig. 2B, region 1). These different conformations result in a variance in position between equivalent Cα atoms of up to 8 Å (Fig. 2B, region 1). However, these regions participate in crystal packing in both HeV-G and NiV-G structures, and there is a potential that the lattice environments may contribute to their different conformations (although within the HeV-G crystal there are four molecules in the crystallographic asymmetric unit which, by definition, make different contacts). Therefore, the two very distinct conformational states exhibited by the two viral proteins may not be strongly characteristic of the individual viruses but rather reflect sampling of the wider conformational space available to these proteins prior to attachment.

A second region of HeV-G that exhibits significant conformational differences to NiV-G occurs between residues Leu202 through Val215 (Fig. 2B and 2C, region 2), where equivalent Cα atoms deviate by up to 9 Å. This part of the structure lies away from the EFN-binding face and is positioned on the β6 and β1 blades of the β-propeller. The two different conformations may be explained by packing interactions which occur between each of the two pairs of adjacent HeV-G molecules in the asymmetric unit. These interactions occlude over 800 $Å^2$ (33) of surface from each HeV-G molecule and result in the generation of a small, two-stranded antiparallel β-sheet (Thr206-Pro208) (Fig. 2B and 2C, region 2) not observed in any of the previously reported receptor-bound or unbound HNV-G structures. However, among all HNV-G structures, this region exhibits conformational plasticity (Fig. 2B and C, region 2), high *B* factors, or in some cases is completely disordered. The intersubunit interactions may therefore be required to order this region.

Conserved mode of assembly. Although the identification of oligomeric states within crystal structures cannot formally prove the mode of oligomerization occurring within the intact virus, such packing interactions can suggest a potential mode of oligomerization. The shared dimeric packing interactions observed in the paramyxovirus attachment glycoproteins are illustrated in Fig. 3. The two dimers observed in the HeV-G crystal structure, although unlikely to represent a biological tetramer, are highly similar (0.2-Å RMS deviation of equivalent Cα positions over the 835 residues of the dimer). The mode of oligomerization for the putative dimers of HeV-G agrees with previous predictions (10, 58, 59) and is strikingly similar to the interactions observed for several other paramyxovirus attachment glycoproteins, including NDV-HN (13), PIV3-HN (35), PIV5-HN (59), and MV-H (12,

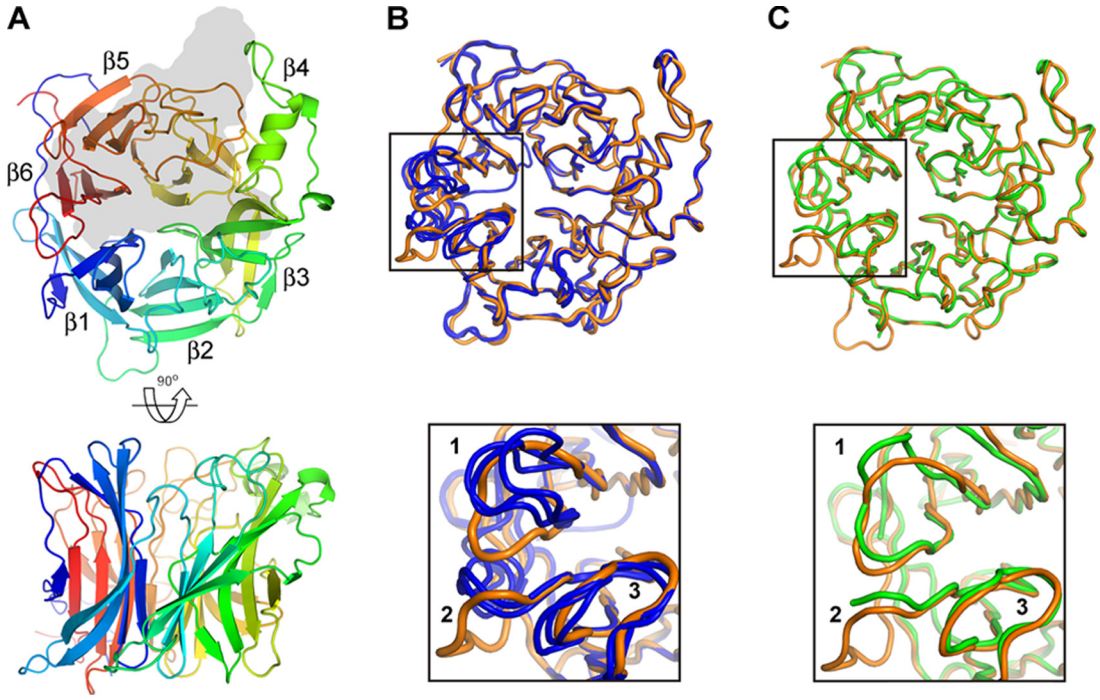

FIG. 2. Crystal structure of unbound HeV-G. (A) Two views of a cartoon diagram of HeV-G colored as a rainbow with the N terminus in blue and the C terminus in red. Blades of the β-propeller are numbered from one to six. The shaded region corresponds to the region of HeV-G that interacts with EFNB2. (B) A Cα trace of a representative HeV-G molecule from the crystallographic asymmetric unit (orange) superposed onto the three available structures of unbound NiV-G molecules (PDB accession no. 2VWD and 3D11) (blue). (C) A Cα trace of a representative unbound HeV-G molecule (orange) superposed onto a representative HeV-G molecule from the HeV-G-EFNB2 structure (PDB accession no. 2VSK) (green). In panels B and C, the boxes in the top panels represent the areas boxed below. The Glu579-Pro590 loop, the region of the Thr206-Pro208 interface strand, and the Lys236-Ala245 loop are labeled 1, 2, and 3, respectively.

31, 48) (Fig. 3B and D), strongly supporting the hypothesis that the mode of dimerization of attachment glycoproteins is conserved between the henipa-, avula-, respiro-, rubula-, and morbilliviruses. Although the total buried surface is less than half of that observed in NDV-HN, PIV3-HN, and PIV5-HN structures (average buried surface of approximately 1,800 Å^2) (Table 2), the location of the dimeric HeV-G association and the overall surface complementarity (36) of the dimer interface is comparable (average dimer surface complementarity score of 0.63 and 0.67 for HeV-G and other paramyxovirus-HN structures, respectively) (Table 2). Analysis of the relative orientations of the two propeller domains in each dimer using SHP (50) shows that for all five viruses there is a very close to exact 2-fold relationship between the two subunits; however, the relative orientations nevertheless differ significantly (Fig. 3B and C). Thus, the three sugar binding attachment proteins (from NDV, PIV3, and PIV5) are closely similar, but if we superpose one of the two subunits on a subunit of the HeV-G dimer then rotations of between 31° and 42° are required to superpose the second on the matching HeV-G subunit (Table 2). MV-H is even more of an outlier, lying some 63° away from the HeV orientation and no closer to the sialic acid binders (Fig. 3D; Table 2). We note also that the glycan binders form dimers with much more contact surface than the protein binders (Table 2). Our observations confirm those of Yuan et al. (58), who noted some flexibility in the subunit orientation of PIV5 but suggest that further rearrangements have evolved to correctly accommodate the more bulky, and perhaps more rigidly presented, protein receptors.

The orientation of the two HeV-G subunits in the dimer is such that when an EFNB2 molecule is docked onto the EFN-binding site of each propeller it does not preclude the formation of the HeV-G dimer. Furthermore, the N-terminal stalk regions would extend in similar directions away from the EFN-binding face, consistent with interstalk disulfide bonding which has been reported to be responsible for HeV-G dimerization and tetramerization (4). While the N-terminal stalk domains of paramyxovirus attachment glycoproteins drive oligomerization (4, 7, 37, 41, 47, 53, 58), homodimers and homotetramers have also been observed in crystallographic analyses of isolated β-propeller domains. Packing interactions in the crystal structures of NDV-HN, PIV3-HN, and MV-H reveal dimeric and tetrameric arrangements (12, 13, 31, 35, 48). These observations demonstrated that the detection of oligomeric states within the crystal lattice is not necessarily precluded by the absence of the stalk domain.

A tetramer composed of two dimers was also observed in the structure of PIV5-HN (59). The glycoprotein used in that study contained the oligomerization-inducing stalk domain. Although this region was disordered in the structure, its presence in the construct used for crystallization suggests that the mode of oligomerization of the globular, receptor binding domains resemble that occurring on the virion. As the dimers observed in the crystal structure of PIV5-HN resemble those of NDV-HN, PIV3-HN, MV-H, and HeV-G dimers which lack the stalk (Fig. 3), it is likely that the mode of dimerization observed in the latter are similarly biologically relevant. However, in no

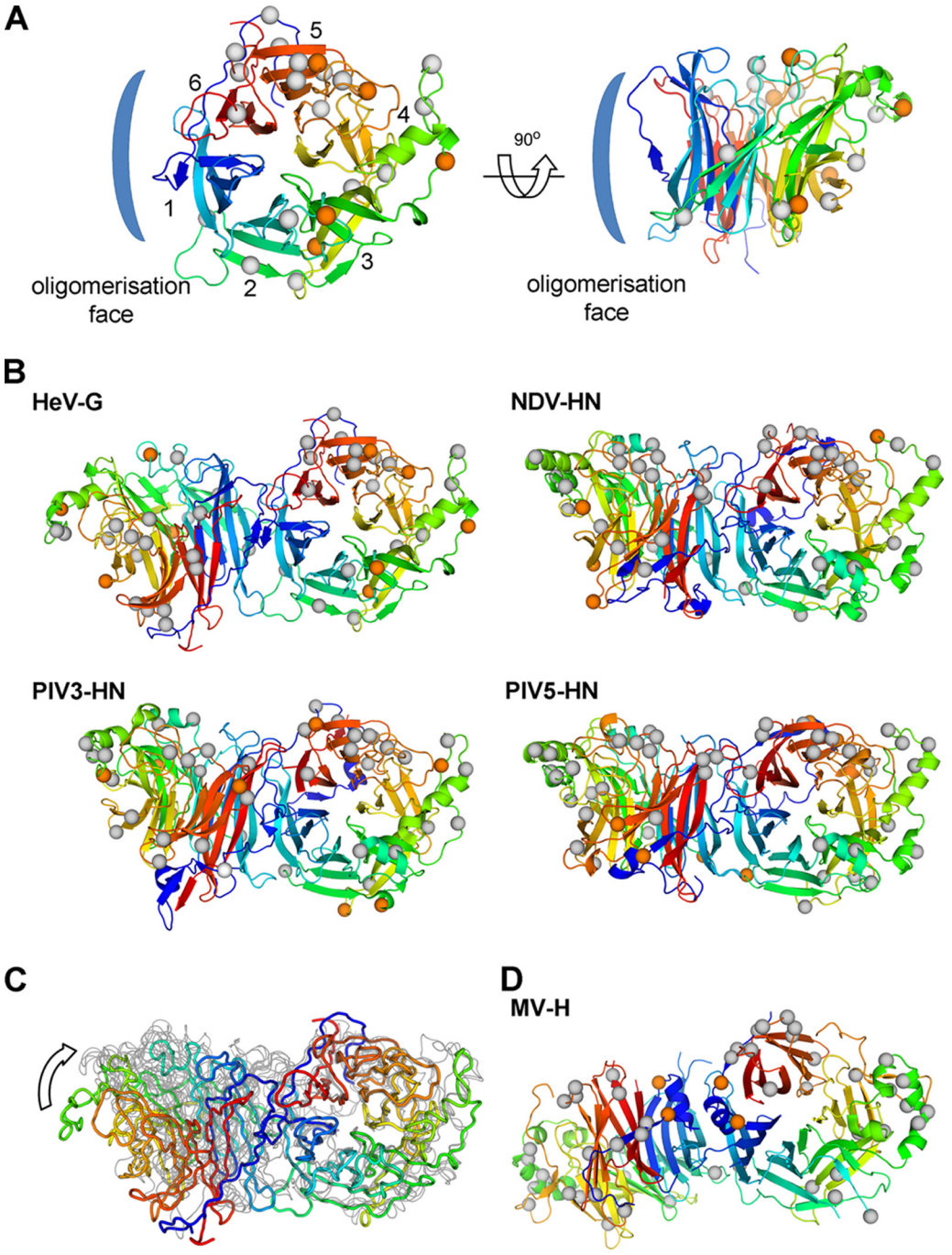

FIG. 3. Prediction of HNV-G oligomerization through mapping of N-linked glycosylation sites. (A) Crystal structure of the HeV-G monomer (cartoon representation) with N-linked glycosylation sites of NiV-G (NCBI sequence no. NP_112027.1), HeV-G (NP_047112.2), PIV1-HN (AAB17174.1), PIV2-HN (BAE95190.1), PIV3-HN (P12562), PIV5-HN (AAB21114.1), Sendai virus-HN (NP_056878.1), and NDV-HN (ABG35959.1) mapped as spheres onto the structure at the equivalent Cα residues [as determined by the NX(S/T)$\bar{X}$ sequon and/or the crystal structure]. The position of the glycans shared between HeV-G and NiV-G are indicated by orange spheres (Asn306, Asn378, Asn417, Asn481, and Asn529). The positions of glycans from the other viruses are indicated by gray spheres. The six-bladed β-propeller is colored as a rainbow, with the N terminus in blue and the C terminus in red. The putative oligomeric interface of Yuan et al. (58) is indicated by a blue bracket. (B) HeV-G dimer and structural comparison with dimers from NDV-HN (PDB accession no. 1E8V), PIV3-HN (PDB accession no. 1V2I), and PIV5-HN (PDB accession no. 1Z4V). All molecules are colored as described for panel A. The glycosylation sites from paramyxoviruses are mapped as spheres onto each of the structures (as for panel A). The positions of glycans which are native to each virus are indicated by orange spheres. The positions of glycans from the other viruses are indicated by gray spheres. (C) The HeV-G dimer and dimers reported in NDV-HN, PIV3-HN, and PIV5-HN crystal structures superposed onto the right HeV-G β-propeller. HeV-G is colored as shown in panel A. All other molecules are colored gray. An arrow is shown to indicate the rotational differences between the nonsuperposed HeV-G and NDV-HN, PIV3-HN, and PIV5-HN β-propeller subunits. (D) The MV-H dimer (PDB accession no. 1E8V) is shown with MV-H glycosylation sites plotted as orange balls. The glycosylation sites identified in panel B are plotted as gray spheres.

TABLE 2. Comparison of HeV-G structure with other paramyxovirus structures

Attachment glycoprotein	PDB accession no.	Surface area buried area in dimer interface (Å^2)	Shape complementarity[e]	Relative angle of association (°)[a]	RMSD[b] (Å [amino acid equivalences])	Sequence identity (%)
HeV-G	2X9M	880[c]	0.63	0	0.3 (415)[c]	100
NiV-G	2VWD	NA[d]	NA	NA	1.1 (410)	81
NDV-HN	1E8V	1,800	0.76	36	2.2 (349)	17
PIV3-HN	1V2I	1,780	0.58	31	2.2 (368)	21
SV5-HN	1Z4V	1,810	0.66	42	2.1 (353)	19
MV-H	3INB	1,070	0.52	63	3.2 (301)	12

[a] Residual angle required to realign subunit B on HeV-G B after superposing the A-B dimer to align subunit A with HeV-G A.
[b] RMSD, root mean square deviation between HeV-G and other β-propeller subunits.
[c] Between equivalent HeV-G monomers in the asymmetric unit.
[d] NA, no apparent dimers were observed in the NiV-G crystal structure.
[e] The statistic for shape complementarity between protein-protein interfaces has been defined by Lawrence et al. (36). The maximum value for perfectly complementary surfaces is 1.

NiV-G or HeV-G crystal structure is there any evidence for tetramer (dimer-of-dimers) formation, as was observed in the crystals of NDV-HN (60) and PIV5-HN (59). Additionally, we note that no putative dimers were observed in the crystal structure of NiV-G alone, or the HeV-G-EFNB2, NiV-G-EFNB2, and NiV-G-EFNB3 complexes (7, 10, 57), indicating that weak interdomain interactions are not observed in all crystals.

Glycosylation of HeV-G. Analysis of the superposed crystal structures of HN from PIV5, NDV, and PIV3 (59) led Yuan et al. to predict the oligomerization interface. It was assumed that the mode of oligomerization would be conserved among paramyxovirus attachment glycoproteins and that these regions would exhibit low divergence in structure. We previously widened this analysis by including the crystal structure of NiV-G and extended the structural analysis by considering the locations of N-linked glycosylation sequons from across the *Paramyxoviridae* family onto the β-propeller fold (10). Glycosylation sites are not usually found at oligomerization interfaces. Mapping the glycosylation sequons from across the *Paramyxoviridae* family onto the β-propeller fold of unliganded NiV-G did not obscure the putative oligomerization interface (10). We have applied this analysis to the structure of the HeV-G monomer reported herein (Fig. 3A). A total of 24 positions of N-linked glycosylation sequons were detected upon sequence alignment across the β-propeller domains of the attachment glycoproteins of NiV, HeV, PIV1, PIV2, PIV3, PIV5, Sendai virus, and NDV (Fig. 3B). Mapping of these glycan sites onto the structure of our crystallographic dimer of HeV-G, and onto the dimers of NDV-HN (13), PIV3-HN (35), and PIV5-HN (59), reveal that they are located away from the dimer interface (Fig. 3B). This same analysis was applied to the more distantly related MV-H (7, 12, 31, 48) and shows a similar arrangement of glycans sitting away from the dimer interface (Fig. 3D); however, two glycans native to MV-H (Asn200 and Asn215) are located in closer proximity to the MV-H dimer interface but do not interfere with the dimeric interface. This provides further support for the physiological relevance of the dimer-of-dimers model of oligomer formation in which the surfaces of the β1- and β6-propellers of HNV-G form one dimerization interface.

Glycosylation of oligomeric HeV-G. The analysis of oligomerization interfaces by consideration of the positions of the glycosylation sequons rests on the assumption that large N-linked glycans are unlikely to be located at the oligomeric interface of the attachment glycoprotein. However, glycans can occur at subunit interfaces of glycoproteins and immobilized glycans at dimer interfaces have been detected upon crystallographic analysis (24). Immobilized glycans that exhibit significant interactions with a protein surface are usually protected from α-mannosidase processing and remain as oligomannose-type glycans (16). Therefore, to assess the validity of our use of glycosylation sequons to identify putative oligomerization interfaces, we performed MALDI-TOF and electrospray-MS analysis on the N-linked glycans of HeV-G_{ecto} and HeV-G_{β} to determine if any glycan was protected from glycosylation processing upon oligomerization (Fig. 3; Table 3). In addition to compositional analysis by MALDI-TOF MS (Fig. 4; Table 3), glycans were structurally analyzed by ion collision-induced dissociation (CID) MS/MS, and the full assignments of the spectra are presented in the supplemental material.

The location of the N-linked glycosylation sites are conserved between HeV-G_{β} and NiV-G_{β}. MALDI-MS analysis of the HeV-G_{β} glycans showed very similar profiles to those previously reported for NiV-G_{β} (10) and other viral glycoproteins (9) recombinantly expressed in HEK 293T cells using the pHLsec vector (3). This indicates that no pronounced protein-directed glycosylation processing was occurring. However, MALDI-TOF MS analysis of HeV-G_{ecto} demonstrated that the specific abundances of the complex-type glycans were altered. Specifically, levels of galactosylation were reduced, suggesting that oligomerization had influenced the accessibility of the N-linked glycans (Fig. 4; Table 3). The sensitivity of β1→4 galactosyltransferase to the structural environment of glycosylation sites has been observed in the processing of IgG glycans. Interdomain glycans of the IgG Fc domain exhibit partial galactosylation, whereas glycosylation occurring in the complementarity-determining regions of the Fab exhibit higher levels of galactosylation (40). Interestingly, alanine-scanning mutagenesis of the stalk region of HeV-G was shown to influence glycan processing, as assessed by mobility on SDS-PAGE (4). These mutations did not seem to disrupt oligomerization of HeV-G but led to disruption of functional interactions with coexpressed HeV-F (4). Overall, these previously reported mutagenesis effects combined with our MS data suggest that glycan processing of HeV-G is sensitive to its oligomerization state and functional assembly.

TABLE 3. MALDI-MS of N-linked glycans from HeV-G_{ecto} and HeV-G_{β}[a]

Peak[b]	$[M+Na]^+$ (*m*/*z*)			Composition			
	Found[c]		Calculated[c]				
	HeV-G_{ecto}	HeV-G_{β}		Hex	HexNAc	dHex	Neu5Ac
1	1,282.5		1,282.5	3	3	1	0
2	1,339.5		1,339.5	3	4	0	0
3	1,403.5		1,403.5	5	2	1	0
4	1,444.5	1,444.5	1,444.5	4	3	1	0
5	1,485.5	1,485.5	1,485.5	3	4	1	0
6	1,501.4	1,501.4	1,501.5	4	4	0	0
7	1,542.5	1,542.5	1,542.6	3	5	0	0
8	1,606.4	1,606.4	1,606.6	5	3	1	0
9	1,647.5	1,647.5	1,647.6	4	4	1	0
10	1,663.5	1,663.5	1,663.6	5	4	0	0
11	1,688.5	1,688.5	1,688.6	3	5	1	0
12	1,704.6		1,704.6	4	5	0	0
13	1,768.6		1,768.6	6	3	1	0
14	1,793.5	1,793.5	1,793.6	4	4	2	1
15	1,809.5	1,809.5	1,809.6	5	4	1	0
16	1,850.4	1,850.4	1,850.7	4	5	1	0
17	1,866.5	1,866.5	1,866.7	5	5	0	0
18	1,891.4	1,891.4	1,891.7	3	6	1	0
19	1,906.0[d]	1,906.0[d]	1,906.7[d]	9	2	0	0
20	1,955.5	1,955.5	1,955.7	5	4	2	0
21	1,971.4	1,971.4	1,971.7	6	4	1	0
22	1,996.4	1,996.4	1,996.7	4	5	2	0
23	2,012.4	2,012.4	2,012.7	5	5	1	0
24	2,053.3	2,053.3	2,053.7	4	6	1	0
25	2,082.3		2,082.7	6	3	1	1 (Na)
26	2,100.4		2,100.8	4	7	0	1 (Na)
27	2,123.3	2,123.3	2,123.7	5	4	1	1 (Na)
28	2,158.4	2,158.4	2,158.8	5	5	2	0
29	2,174.2	2,174.2	2,174.8	6	5	1	0
30	2,215.4		2,215.8	5	6	1	0
31		2,245.2	2,245.7	5	4	0	2
32		2,267.3	2,267.8	5	4	0	2 (Na)
33		2,303.2	2,303.8	5	5	1	0
34	2,325.3	2,325.3	2,325.8	5	5	1	1 (Na)
35	2,377.2	2,377.2	2,377.9	6	6	1	0

[a] An extended MS table is available in the supplemental material.
[b] Peak ID corresponds to ions identified by MALDI-MS (Fig. 4).
[c] Monoisotopic mass except where indicated.
[d] Avg mass.

Despite the reduction in glycosyltransferase processing of HeV-G_{ecto}, only trace levels of oligomannose-type glycans were detected, confirming that all glycan sites are accessible to α-mannosidase processing when expressed as an oligomer. These data confirm that glycosylation sites on HNV-G are unlikely to significantly contribute to the buried surface area of the oligomerization interface, further supporting our hypothesis that the oligomerization interfaces are predicted by the paucity of glycosylation sequons.

Conclusions. Our crystallographic analysis of henipaviral attachment glycoproteins has demonstrated plasticity in many regions of the ephrin-binding loops. Understanding the conformations explored by unliganded viral attachment glycoproteins will inform the design of templates for rational drug discovery. The modest success of structure-based drug design in the identification of compounds that specifically disrupt target protein-protein interactions has been suggested to be, to some extent, explained by the limited conformational space defined by the template (55). We anticipate that knowledge of the structures of both unliganded and receptor-bound conformations will be necessary for more robust *de novo* computational screening of small-molecule libraries and for structure-based optimization of lead antiviral compounds.

From the detailed crystallographic analysis of isolated henipavirus attachment glycoproteins to the low-resolution electron microscopic analysis of intact virions, there is a paucity of information of the architecture of the attachment and fusion assembly. In accord with Yuan et al. (58), we have suggested a mode of oligomerization of HeV-G based upon the packing interactions within our crystal structure as well as the interactions of related paramyxovirus structures but find that this association is significantly reconfigured for those viruses which

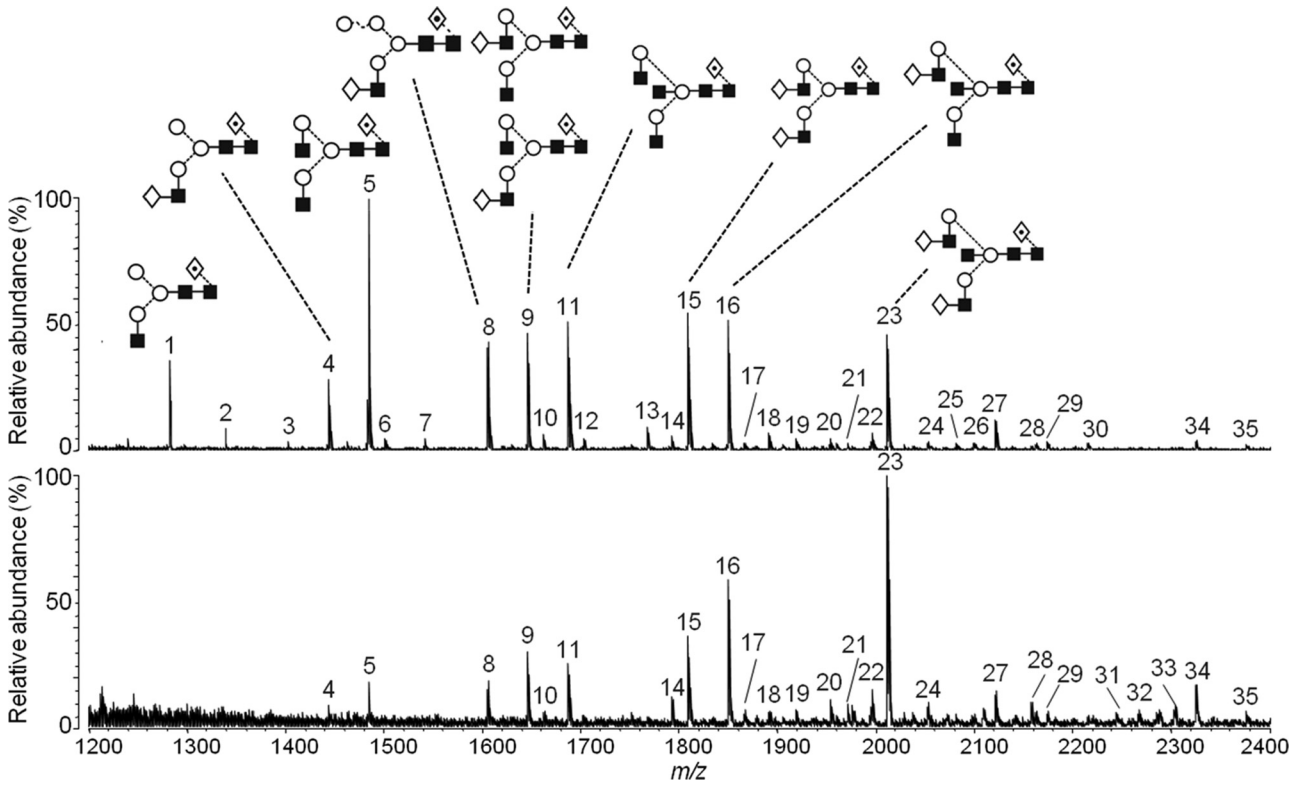

FIG. 4. MALDI-MS analysis of N-linked glycans from oligomeric HeV-G_{ecto} (top panel) and HeV-G_{β} (bottom panel) expressed in HEK 293T cells. Monosaccharide compositions of the numbered peaks are presented in Table 3. Structures were assigned by electrospray ionization-MS/MS (see Table S1 in the supplemental material). Cartoon representations of the structures are shown for peaks with greater than 20% relative abundance (peak 9 exhibits two predominant isomeric forms). Diamond, Gal; filled square, GlcNAc; open circle, Man; diamond with black dot, Fuc (29). The linkage position is shown by the angle of the lines linking the sugar residues (vertical line, 2-link; forward slash, 3-link; horizontal line, 4-link; back slash, 6-link). Anomericity is indicated by unbroken lines for β bonds and broken lines for α bonds (29).

bind protein receptors. This analysis has supported the notion that information on low-affinity interactions can be gleaned by the analysis of modes of crystal packing. Understanding the intermolecular interactions of the attachment glycoproteins is likely to be a prerequisite for a full structural description of viral attachment and fusion.

ACKNOWLEDGMENTS

We are grateful for the help of W. Lu for the tissue culture, K. Harlos for data collection, and the staff of Beamline ID23.2 at the European Synchrotron Radiation Facility for assistance. We thank C. N. Scanlan for access to the Shimazu AXIMA performance MALDI-TOF/TOF mass spectrometer funded by the International AIDS Vaccine Initiative (IAVI).

D.I.S. is an MRC Professor of Structural Biology, E.Y.J. is a Cancer Research UK Principal Research Fellow, T.A.B. is a Sir Henry Wellcome Postdoctoral Fellow, and M.C. is a Fellow of Oriel College, Oxford, United Kingdom.

This work was funded by the Wellcome Trust (075491/Z/04), Medical Research Council, Cancer Research UK, the Oxford Glycobiology Institute, and Spine2 Complexes (FP6-RTD-031220).

REFERENCES

1. **Aguilar, H. C., Z. A. Ataman, V. Aspericueta, A. Q. Fang, M. Stroud, O. A. Negrete, R. A. Kammerer, and B. Lee.** 2009. A novel receptor-induced activation site in the Nipah virus attachment glycoprotein (G) involved in triggering the fusion glycoprotein (F). J. Biol. Chem. **284:**1628–1635.
2. **Alymova, I. V., G. Taylor, and A. Portner.** 2005. Neuraminidase inhibitors as antiviral agents. Curr. Drug Targets Infect. Disord. **5:**401–409.
3. **Aricescu, A. R., W. Lu, and E. Y. Jones.** 2006. A time- and cost-efficient system for high-level protein production in mammalian cells. Acta Crystallogr. D Biol. Crystallogr. **62:**1243–1250.
4. **Bishop, K. A., A. C. Hickey, D. Khetawat, J. R. Patch, K. N. Bossart, Z. Zhu, L. F. Wang, D. S. Dimitrov, and C. C. Broder.** 2008. Residues in the stalk domain of the Hendra virus G glycoprotein modulate conformational changes associated with receptor binding. J. Virol. **82:**11398–11409.
5. **Börnsen, K. O., M. D. Mohr, and H. M. Widmer.** 1995. Ion exchange and purification of carbohydrates on a Nafion membrane as a new sample pretreatment for matrix-assisted laser desorption-ionization mass spectrometry. Rapid Commun. Mass Spectrom. **9:**1031–1034.
6. **Bossart, K. N., G. Crameri, A. S. Dimitrov, B. A. Mungall, Y. R. Feng, J. R. Patch, A. Choudhary, L. F. Wang, B. T. Eaton, and C. C. Broder.** 2005. Receptor binding, fusion inhibition, and induction of cross-reactive neutralizing antibodies by a soluble G glycoprotein of Hendra virus. J. Virol. **79:**6690–6702.
7. **Bowden, T. A., A. R. Aricescu, R. J. Gilbert, J. M. Grimes, E. Y. Jones, and D. I. Stuart.** 2008. Structural basis of Nipah and Hendra virus attachment to their cell-surface receptor ephrin-B2. Nat. Struct. Mol. Biol. **15:**567–572.
8. **Bowden, T. A., A. R. Aricescu, J. E. Nettleship, C. Siebold, N. Rahman-Huq, R. J. Owens, D. I. Stuart, and E. Y. Jones.** 2009. Structural plasticity of eph receptor A4 facilitates cross-class ephrin signaling. Structure **17:**1386–1397.
9. **Bowden, T. A., M. Crispin, S. C. Graham, D. J. Harvey, J. M. Grimes, E. Y. Jones, and D. I. Stuart.** 2009. Unusual molecular architecture of the Machupo virus attachment glycoprotein. J. Virol. **83:**8259–8265.
10. **Bowden, T. A., M. Crispin, D. J. Harvey, A. R. Aricescu, J. M. Grimes, E. Y. Jones, and D. I. Stuart.** 2008. Crystal structure and carbohydrate analysis of Nipah virus attachment glycoprotein: a template for antiviral and vaccine design. J. Virol. **82:**11628–11636.
11. **Chang, V. T., M. Crispin, A. R. Aricescu, D. J. Harvey, J. E. Nettleship, J. A. Fennelly, C. Yu, K. S. Boles, E. J. Evans, D. I. Stuart, R. A. Dwek, E. Y. Jones, R. J. Owens, and S. J. Davis.** 2007. Glycoprotein structural genomics: solving the glycosylation problem. Structure **15:**267–273.
12. **Colf, L. A., Z. S. Juo, and K. C. Garcia.** 2007. Structure of the measles virus hemagglutinin. Nat. Struct. Mol. Biol. **14:**1227–1228.
13. **Crennell, S., T. Takimoto, A. Portner, and G. Taylor.** 2000. Crystal structure

of the multifunctional paramyxovirus hemagglutinin-neuraminidase. Nat. Struct. Biol. **7:**1068–1074.
14. **Crispin, M., T. A. Bowden, C. H. Coles, K. Harlos, A. R. Aricescu, D. J. Harvey, D. I. Stuart, and E. Y. Jones.** 2009. Carbohydrate and domain architecture of an immature antibody glycoform exhibiting enhanced effector functions. J. Mol. Biol. **387:**1061–1066.
15. **Crispin, M., D. J. Harvey, V. T. Chang, C. Yu, A. R. Aricescu, E. Y. Jones, S. J. Davis, R. A. Dwek, and P. M. Rudd.** 2006. Inhibition of hybrid and complex-type glycosylation reveals the presence of the GlcNAc transferase I-independent fucosylation pathway. Glycobiology **16:**748–756.
16. **Crispin, M. D., G. E. Ritchie, A. J. Critchley, B. P. Morgan, I. A. Wilson, R. A. Dwek, R. B. Sim, and P. M. Rudd.** 2004. Monoglucosylated glycans in the secreted human complement component C3: implications for protein biosynthesis and structure. FEBS Lett. **566:**270–274.
17. **Davis, I. W., A. Leaver-Fay, V. B. Chen, J. N. Block, G. J. Kapral, X. Wang, L. W. Murray, W. B. Arendall III, J. Snoeyink, J. S. Richardson, and D. C. Richardson.** 2007. MolProbity: all-atom contacts and structure validation for proteins and nucleic acids. Nucleic Acids Res. **35:**W375–383.
18. **Dörig, R. E., A. Marcil, A. Chopra, and C. D. Richardson.** 1993. The human CD46 molecule is a receptor for measles virus (Edmonston strain). Cell **75:**295–305.
19. **Drexler, J. F., V. M. Corman, F. Gloza-Rausch, A. Seebens, A. Annan, A. Ipsen, T. Kruppa, M. A. Muller, E. K. Kalko, Y. Adu-Sarkodie, S. Oppong, and C. Drosten.** 2009. Henipavirus RNA in African bats. PLoS One **4:**e6367.
20. **Eaton, B. T., C. C. Broder, D. Middleton, and L. F. Wang.** 2006. Hendra and Nipah viruses: different and dangerous. Nat. Rev. Microbiol. **4:**23–35.
21. **Elbein, A. D., J. E. Tropea, M. Mitchell, and G. P. Kaushal.** 1990. Kifunensine, a potent inhibitor of the glycoprotein processing mannosidase I. J. Biol. Chem. **265:**15599–15605.
22. **Emsley, P., and K. Cowtan.** 2004. Coot: model-building tools for molecular graphics. Acta Crystallogr. D Biol. Crystallogr. **60:**2126–2132.
23. **Field, H. E., P. C. Barratt, R. J. Hughes, J. Shield, and N. D. Sullivan.** 2000. A fatal case of Hendra virus infection in a horse in north Queensland: clinical and epidemiological features. Aust. Vet. J. **78:**279–280.
24. **Fusetti, F., K. H. Schroter, R. A. Steiner, P. I. van Noort, T. Pijning, H. J. Rozeboom, K. H. Kalk, M. R. Egmond, and B. W. Dijkstra.** 2002. Crystal structure of the copper-containing quercetin 2,3-dioxygenase from *Aspergillus japonicus*. Structure **10:**259–268.
25. **Harvey, D. J.** 2005. Fragmentation of negative ions from carbohydrates: part 1. Use of nitrate and other anionic adducts for the production of negative ion electrospray spectra from N-linked carbohydrates. J. Am. Soc. Mass Spectrom. **16:**622–630.
26. **Harvey, D. J.** 2005. Fragmentation of negative ions from carbohydrates: part 2. Fragmentation of high-mannose N-linked glycans. J. Am. Soc. Mass Spectrom. **16:**631–646.
27. **Harvey, D. J.** 2005. Fragmentation of negative ions from carbohydrates: part 3. Fragmentation of hybrid and complex N-linked glycans. J. Am. Soc. Mass Spectrom. **16:**647–659.
28. **Harvey, D. J.** 2005. Structural determination of N-linked glycans by matrix-assisted laser desorption/ionization and electrospray ionization mass spectrometry. Proteomics **5:**1774–1786.
29. **Harvey, D. J., A. H. Merry, L. Royle, M. P. Campbell, R. A. Dwek, and P. M. Rudd.** 2009. Proposal for a standard system for drawing structural diagrams of N- and O-linked carbohydrates and related compounds. Proteomics **9:**3796–3801.
30. **Harvey, D. J., L. Royle, C. M. Radcliffe, P. M. Rudd, and R. A. Dwek.** 2008. Structural and quantitative analysis of N-linked glycans by matrix-assisted laser desorption ionization and negative ion nanospray mass spectrometry. Anal. Biochem. **376:**44–60.
31. **Hashiguchi, T., M. Kajikawa, N. Maita, M. Takeda, K. Kuroki, K. Sasaki, D. Kohda, Y. Yanagi, and K. Maenaka.** 2007. Crystal structure of measles virus hemagglutinin provides insight into effective vaccines. Proc. Natl. Acad. Sci. U. S. A. **104:**19535–19540.
32. **Hooper, P. T., A. R. Gould, A. D. Hyatt, M. A. Braun, J. A. Kattenbelt, S. G. Hengstberger, and H. A. Westbury.** 2000. Identification and molecular characterization of Hendra virus in a horse in Queensland. Aust. Vet. J. **78:**281–282.
33. **Krissinel, E., and K. Henrick.** 2007. Inference of macromolecular assemblies from crystalline state. J. Mol. Biol. **372:**774–797.
34. **Küster, B., S. F. Wheeler, A. P. Hunter, R. A. Dwek, and D. J. Harvey.** 1997. Sequencing of N-linked oligosaccharides directly from protein gels: in-gel deglycosylation followed by matrix-assisted laser desorption/ionization mass spectrometry and normal-phase high-performance liquid chromatography. Anal. Biochem. **250:**82–101.
35. **Lawrence, M. C., N. A. Borg, V. A. Streltsov, P. A. Pilling, V. C. Epa, J. N. Varghese, J. L. McKimm-Breschkin, and P. M. Colman.** 2004. Structure of the haemagglutinin-neuraminidase from human parainfluenza virus type III. J. Mol. Biol. **335:**1343–1357.
36. **Lawrence, M. C., and P. M. Colman.** 1993. Shape complementarity at protein/protein interfaces. J. Mol. Biol. **234:**946–950.
37. **Markwell, M. A., and C. F. Fox.** 1980. Protein-protein interactions within paramyxoviruses identified by native disulfide bonding or reversible chemical cross-linking. J. Virol. **33:**152–166.
38. **McCoy, A. J., R. W. Gross-Kunstleve, P. D. Adams, M. D. Winn, L. C. Storoni, and R. J. Read.** 2007. Phaser crystallographic software. J. Appl. Cryst. **40:**658–674.
39. **McEachern, J. A., J. Bingham, G. Crameri, D. J. Green, T. J. Hancock, D. Middleton, Y. R. Feng, C. C. Broder, L. F. Wang, and K. N. Bossart.** 2008. A recombinant subunit vaccine formulation protects against lethal Nipah virus challenge in cats. Vaccine **26:**3842–3852.
40. **Mimura, Y., P. R. Ashton, N. Takahashi, D. J. Harvey, and R. Jefferis.** 2007. Contrasting glycosylation profiles between Fab and Fc of a human IgG protein studied by electrospray ionization mass spectrometry. J. Immunol. Methods **326:**116–126.
41. **Morrison, T. G.** 1988. Structure, function, and intracellular processing of paramyxovirus membrane proteins. Virus Res. **10:**113–135.
42. **Murray, K., P. Selleck, P. Hooper, A. Hyatt, A. Gould, L. Gleeson, H. Westbury, L. Hiley, L. Selvey, B. Rodwell, et al.** 1995. A morbillivirus that caused fatal disease in horses and humans. Science **268:**94–97.
43. **Murshudov, G. N., A. A. Vagin, and E. J. Dodson.** 1997. Refinement of macromolecular structures by the maximum-likelihood method. Acta Crystallogr. D Biol. Crystallogr. **53:**240–255.
44. **Naniche, D., G. Varior-Krishnan, F. Cervoni, T. F. Wild, B. Rossi, C. Rabourdin-Combe, and D. Gerlier.** 1993. Human membrane cofactor protein (CD46) acts as a cellular receptor for measles virus. J. Virol. **67:**6025–6032.
45. **Otwinowski, A., and W. Minor.** 1997. Processing of X-ray diffraction data collected in oscillation mode, p. 307–326. *In* C. W. Carter, Jr., and R. M. Sweet (ed.), Methods in enzymology, vol. 276. Academic Press, New York, NY.
46. **Parashar, U. D., L. M. Sunn, F. Ong, A. W. Mounts, M. T. Arif, T. G. Ksiazek, M. A. Kamaluddin, A. N. Mustafa, H. Kaur, L. M. Ding, G. Othman, H. M. Radzi, P. T. Kitsutani, P. C. Stockton, J. Arokiasamy, H. E. Gary, Jr., and L. J. Anderson.** 2000. Case-control study of risk factors for human infection with a new zoonotic paramyxovirus, Nipah virus, during a 1998–1999 outbreak of severe encephalitis in Malaysia. J. Infect. Dis. **181:**1755–1759.
47. **Parks, G. D., and R. A. Lamb.** 1990. Folding and oligomerization properties of a soluble and secreted form of the paramyxovirus hemagglutinin-neuraminidase glycoprotein. Virology **178:**498–508.
48. **Santiago, C., M. L. Celma, T. Stehle, and J. M. Casasnovas.** 2010. Structure of the measles virus hemagglutinin bound to the CD46 receptor. Nat. Struct. Mol. Biol. **17:**124–129.
49. **Selvey, L. A., R. M. Wells, J. G. McCormack, A. J. Ansford, K. Murray, R. J. Rogers, P. S. Lavercombe, P. Selleck, and J. W. Sheridan.** 1995. Infection of humans and horses by a newly described morbillivirus. Med. J. Aust. **162:**642–645.
50. **Stuart, D. I., M. Levine, H. Muirhead, and D. K. Stammers.** 1979. Crystal structure of cat muscle pyruvate kinase at a resolution of 2.6 Å. J. Mol. Biol. **134:**109–142.
51. **Tatsuo, H., N. Ono, K. Tanaka, and Y. Yanagi.** 2000. SLAM (CDw150) is a cellular receptor for measles virus. Nature **406:**893–897.
52. **Tatsuo, H., N. Ono, and Y. Yanagi.** 2001. Morbilliviruses use signaling lymphocyte activation molecules (CD150) as cellular receptors. J. Virol. **75:**5842–5850.
53. **Thompson, S. D., W. G. Laver, K. G. Murti, and A. Portner.** 1988. Isolation of a biologically active soluble form of the hemagglutinin-neuraminidase protein of Sendai virus. J. Virol. **62:**4653–4660.
54. **Walter, T. S., J. M. Diprose, C. J. Mayo, C. Siebold, M. G. Pickford, L. Carter, G. C. Sutton, N. S. Berrow, J. Brown, I. M. Berry, G. B. Stewart-Jones, J. M. Grimes, D. K. Stammers, R. M. Esnouf, E. Y. Jones, R. J. Owens, D. I. Stuart, and K. Harlos.** 2005. A procedure for setting up high-throughput nanolitre crystallization experiments. Crystallization workflow for initial screening, automated storage, imaging and optimization. Acta Crystallogr. D Biol. Crystallogr. **61:**651–657.
55. **Wells, J. A., and C. L. McClendon.** 2007. Reaching for high-hanging fruit in drug discovery at protein-protein interfaces. Nature **450:**1001–1009.
56. **Winn, M. D., G. N. Murshudov, and M. Z. Papiz.** 2003. Macromolecular TLS refinement in REFMAC at moderate resolutions. Methods Enzymol. **374:**300–321.
57. **Xu, K., K. R. Rajashankar, Y. P. Chan, J. P. Himanen, C. C. Broder, and D. B. Nikolov.** 2008. Host cell recognition by the henipaviruses: crystal structures of the Nipah G attachment glycoprotein and its complex with ephrin-B3. Proc. Natl. Acad. Sci. U. S. A. **105:**9953–9958.
58. **Yuan, P., G. P. Leser, B. Demeler, R. A. Lamb, and T. S. Jardetzky.** 2008. Domain architecture and oligomerization properties of the paramyxovirus PIV 5 hemagglutinin-neuraminidase (HN) protein. Virology **378:**282–291.
59. **Yuan, P., T. B. Thompson, B. A. Wurzburg, R. G. Paterson, R. A. Lamb, and T. S. Jardetzky.** 2005. Structural studies of the parainfluenza virus 5 hemagglutinin-neuraminidase tetramer in complex with its receptor, sialyllactose. Structure **13:**803–815.
60. **Zaitsev, V., M. von Itzstein, D. Groves, M. Kiefel, T. Takimoto, A. Portner, and G. Taylor.** 2004. Second sialic acid binding site in Newcastle disease virus hemagglutinin-neuraminidase: implications for fusion. J. Virol. **78:**3733–3741.